The influence of wavelength in extinction measurements and beam steering in laser-induced incandescence measurements in sooting flames

Jochen Zerbs, Klaus Peter Geigle*, Oliver Lammel, Joachim Hader, Ronnie Stirn, Redjem Hadef[1], Wolfgang Meier

Institute of Combustion Technology, DLR, Pfaffenwaldring 38-40, 70569 Stuttgart, Germany

[1] BP 297, Institut de Génie Mécanique, Université Larbi Ben M'Hidi, 04000 Oum El Bouaghi, Algeria

*klauspeter.geigle@dlr.de

Tel.: ++49-711-6862-398

Fax: ++49-711-6862-578

Abstract

The accuracy of laser-induced incandescence (LII) measurements is significantly influenced by the calibration process and the laser profile degradation due to beam steering. Additionally, the wavelength used for extinction measurements, needed for LII calibration, is critical and should be kept as high as possible in order to avoid light absorption by molecular species in the flame. The influence of beam steering on the LII measurement was studied in turbulent sooting C_2H_4/air flames at different pressures. While inhomogeneities in the laser profile become smoothed out in time averaged measurements, especially at higher pressure, the corresponding single shot beam profiles reveal an increasing effect of beam steering. In the current configuration it was observed that the resulting local laser fluence remains within certain limits (30% to 200%) of the original value. A sufficiently high incident laser fluence can thus prevent the local fluence from dropping below the LII threshold value of approximately 0.3 J/cm^2 at the cost of increased soot surface vaporization. A spatial resolution in the dimension of the sheet thickness of below 1 mm cannot be guaranteed at increased pressure of 9 bars due to beam steering. A feasibility study in a combustor at technical conditions demonstrates the influence of both effects beam steering and choice of calibration wavelength and led to the conclusion that, however, a shot to shot calibration of LII with simultaneously measured extinction can be realized.

1. Introduction

Laser-induced incandescence (LII) has proven to be a versatile tool for measuring soot distributions quantitatively. The basic concept of this technique lies in the heating of soot particles by a pulsed laser beam up to 4000 K or more and the detection of the particles' radiation (incandescence) intensity. This intensity is under certain conditions [1] linearly correlated with the soot volume fraction. For quantitative data evaluation, a calibration measurement using a different technique is necessary. Two important parameters influencing the accuracy of LII measurements are (1) the calibration process and (2) the laser fluence at the measurement location.

LII is frequently quantified by an absorption-based diagnostic such as line-of-sight extinction [2,3] or cavity ringdown spectroscopy [4,5]. Here, it has to be considered that light absorption in (fuel-rich) flames might not exclusively be caused by soot particles but also by molecular species, e.g. polycyclic aromatic hydrocarbons (PAH). For reason of convenience of light sources and detectors, visible wavelengths have often been employed [2,3,4]. While for certain sooting flames the contribution of PAH to the total absorption in the visible was determined or estimated to be negligible [4,6] others used the difference in absorption at two wavelengths to deduce information on PAH content [5]. In order to contribute to a clarification of this effect, the present study compares line-of-sight extinction measurements at different wavelengths applied to a stable sooting flame. For this purpose we chose a well defined, easily accessible burner which has already been used before as a standard test case within the first international LII workshop [7] and which is documented by a large number of publications describing the use of various different diagnostics (for example [2,8-10]). Thus, the results contribute to an extension of the data base for this burner and also to a better interpretation and assessment of our results obtained at the high-pressure test rig described in this paper.

In high fluence LII measurements, the laser fluence is chosen in a range where the LII signal is insensitive to laser intensity, the so called plateau regime (for example [5]). However, the range of the plateau regime, in terms of laser fluences, is limited, there is a small remaining dependence of the LII signal on laser fluence, and the laser beam geometry is essential. Typically, the exciting laser beam is assumed to cross the turbulent flame environment approximately unchanged or possibly attenuated. Frequently used descriptions of the beam cross-section are Gaussian or top hat, while in reality beam steering might alter the laser profile to an irregular shape and, in addition, which may well alter with passage through the medium. This means that too strong variations of the laser fluence within a laser sheet should be avoided and that effects like beam steering can influence the accuracy of an LII measurement.

Beam steering is caused by gradients of the refractive index and cannot be avoided in flames where large density gradients are present. In turbulent flames the effect is even more pronounced because of turbulent mixing of hot and cold fluid elements and rapidly changing corrugated flame fronts. With increasing pressure and long pathways through the flame, beam steering effects become even more dramatic. Thus, a laser intensity profile can change drastically when passing through a turbulent flame. Publications are available describing this effect and providing algorithms to account for it whenever possible. A characterization of beam steering effects for laser-induced fluorescence [11, 12], CARS [11] and Rayleigh scattering [13] was done recently. Weinberg provides a detailed computation of beam steering emphasizing the effect of increased pressure. The influence of beam steering on applicability of LII, in contrast, has not been studied to date. While the cited Rayleigh experiments allow for ray tracing due to large and relatively homogeneous signal structure and additionally a direct measure of temperature is provided, LII has a strongly non-linear behavior with laser fluence and the soot structures in turbulent flames are typically small exhibiting strong gradients. For fluences close to or below the LII plateau threshold, a differentiation between real soot concentration gradients and signal gradients caused by laser fluence variations is not possible and tracing algorithms fail due to insufficient signal in large parts of the image. Beyond this threshold any fluence variation is hidden by the low dependence of signal intensity upon laser fluence.

Since there is a big interest in using LII for technical combustion processes [14-20], the question about limitations of the technique at these technical conditions must be raised. The application of laser-based diagnostics to combustors operated at high pressure involves several challenges that affect the measurements' precision. It is well known, that the influence

of droplets on the LII signal (i.e. mainly scattering) can be avoided by an adequate choice of excitation and detection wavelengths [16,20,21] and suitable filters. Other issues remain worth consideration.

Of particular significance at increased pressure (as typical for technical combustion) are the uncertainties resulting from turbulence and/or unsteadiness associated with high pressure flames. To explore the influence and magnitude of these factors, tests have been performed in a laboratory combustor at pressures up to 9 bar and in a test rig for technical flames up to 15 bars. These tests provide the opportunity to study the influence of turbulent sooting flames at increased pressure on the laser sheet properties and thus on calibration and spatial resolution in detail.

One standard approach to perform quantitative processing of LII images from technical flames requires a calibration flame of known properties. It is based on soot properties determined in atmospheric sooting flames and the correspondent LII behavior, i.e. signal decay at ambient pressure. Typically, short and prompt detector gates are recommended [7], capturing the temporal peak of the signal but not the long tail. At increasing pressure, conduction from the heated particles to their environment becomes more efficient due to the higher number of collisions, an effect that is reducing the LII signal duration and thus the temporal signal distribution with respect to the detector gate changes. This effect is not accounted for when transferring a calibration done at ambient pressure to a high pressure experiment. To improve the precision of the soot volume fraction measurements, the applicability of a calibration procedure directly performed in the high pressure flame is evaluated. For this purpose, a simultaneous extinction measurement is included into the LII experiment. 2D LII images are correlated on a shot-to-shot basis with a simultaneous laser extinction measurement; correlation of both provides a calibration constant that can be used to quantify LII.

The starting point of the presented experiments was the LII experiment at the technical high pressure combustor. During data analysis we determined a relatively wide scatter of the calibration parameters. This motivated us to study potential sources on a more fundamental, and if possible, quantitative level. The paper starts with the more fundamental studies of quantification of the influence of the extinction wavelength using an atmospheric pressure McKenna burner and of beam steering using a high pressure turbulent flame before using the gained insight for interpretation of the complex LII experiment under technical conditions.

2. Measurement techniques

2.1 Extinction measurements

Soot volume fractions f_v were determined by using the Beer-Lambert law:

$$\log \frac{I}{I_0} = -K_e \frac{f_v}{\lambda} L \tag{1}$$

Here, λ is the wavelength, K_e the dimensionless extinction coefficient and L the length of the absorbing medium. The soot concentration along the optical path is assumed to be constant, an assumption that might not be justified [8] and was not verified in our experiment. Nevertheless, this assumption does not change the results presented but might influence the comparison with literature data [2]. According to eq. (1) the logarithm term correlates with the soot concentration linearly. For non-uniform soot distributions, f_v is replaced by the integral along the optical path and L split into infinitesimal small path elements dl.

While soot absorbs light in a continuous spectral range from UV to IR, molecular species present in flames are selective absorbers. The energy gap for an electronic transition,

3

responsible for the longest wavelength' absorption of a molecule, decreases with the size of the conjugated electronic system. For aromatic species, this upper absorption wavelength increases from approximately 270 nm for benzene over 370 nm for pyrene and 430 nm for coronene up to values above 500 nm [22], while on the other side concentrations of these species in the flame decrease with molecular size. Consequently, the strongest absorption by PAH is observed in the ultraviolet, while decreasing levels of absorption are possible well into the visible when PAH levels are significant.

2.2 Laser-induced incandescence

For low fluence laser-induced incandescence, signal for a given soot concentration is strongly nonlinearly dependent on the exciting laser fluence. Preferably, LII experiments for soot concentration mapping are performed in the plateau region of the LII response, where the LII signal is approximately independent of the laser fluence and only depends on the soot volume fraction. Too high laser fluences are not recommended because that results in increasingly significant modifications of soot morphology and surface vaporization [23,24] while low laser fluences are not sufficient to heat all particles in the probe volume to a uniform temperature close to soot surface vaporization.

The existence and quality of the plateau region depends on the optical set-up (beam shaping elements, beam profile) and gate duration as is exemplified in Fig. 1. Bladh et al. [25] measured the local signal intensity in backward LII correlated to peak fluence for prompt short gate (filled circle) and delayed long gate (open circle) at 1064 nm excitation. Geigle et al. [26] and Axelsson et al. [2] determined the response curve for prompt gate averaging along differently shaped beam thickness at 1064 nm and 532 nm excitation, respectively. These examples present only part of the LII response curves known from literature but reveal a strong dependency on the chosen set-up. The dependency of the plateau regime with beam shape justifies a detailed study of beam steering in application of LII to turbulent flames.

3. Setup

3.1 Extinction measurements in stable reproducible flame using different wavelengths

3.1.1 Optics

The extinction experiments (Fig. 2) were carried out at three different wavelengths using a green diode laser, a Helium Neon laser and an infrared diode laser emitting at 532, 632.8 and 1064 nm, respectively. The laser beams were focused into the flame by a plano-convex f=500 mm lens, collimated behind the flame by a second f=500 mm lens and subsequently focused into the signal photodiode to measure the attenuated intensity I. The back reflection of a neutral glass filter was used to monitor the reference intensity I_0. For the green diode and Helium Neon laser a KG4 filter was placed in front of the signal photodiode to attenuate flame radiation, for the infrared diode the laser beam was redirected onto the detector by a high reflective 1064 nm mirror. Laser intensities were, in the case of the green diode and Helium Neon laser, modulated by a chopper, in the case of the infrared diode a function generator was used to directly modulate the laser. A modulation frequency of 800 and 1000 Hz were used for the chopper and function generator, respectively. A digital oscilloscope averaged over 256 periods and the resulting voltage amplitudes were taken as a measure of I and I_0, a measurement repeated ten times at each location. The value log(I/I_0) was then background corrected by a measurement without flame taken before each run. The distance L was determined by measuring the yellow, luminous part of the flame on a digital photograph at each height above the burner (HAB).

3.1.2 Burner and flames

The investigated ethylene/air flames were stabilized on a stainless steel water-cooled porous plug burner (McKenna, Holthuis & Associates) with a fixed total gas flow of 10 sl/min and an uncertainty of the flow-controller calibration in the range of 1-2 %. Ethylene with a purity of 3.0 was used. The burner consists of a porous plug with a diameter of 60 mm. To prevent flame flickering the flame was stabilized by a cylindrical steel plate with a thickness of 20 mm and a diameter of 60 mm, mounted such that the lower surface was at a height above burner (HAB) of 21 mm. This burner and stabilization geometry has been proposed as a standard test case preparing the first international workshop on LII [7]. The burner was traversed vertically allowing for extinction measurements between HAB=2 and 18 mm. The equivalence ratio Φ was 2.1 and 2.3.

3.2 Beam steering in turbulent lab flames at different pressures

3.2.1 Optics

The optical setup for monitoring beam steering is shown in Fig. 3. For excitation the fundamental wavelength of a Nd:YAG laser with 10 Hz repetition rate and with a pulse duration of 4 ns (Quantel, Brilliant) was employed. A three lens optics consisting of a cylindrical f=-80 mm, a spherical f=1000 mm and second cylindrical f=-300 mm lens formed a parallel laser sheet of approximately 1 mm thickness while a homogeneous, 6 mm high section of the sheet was selected by a rectangular aperture. The transmitted IR laser sheet was 1:1 imaged onto a beam profiler (WinCamD-UCM, Dataray) using a spherical f=500 mm, 50 mm diameter lens, a 9.5 mm thick quartz plate (0.5° wedge) and a suitable set of NG filters.

3.2.2 Burner

The combustor shown in Fig. 4 is a down-scaled version of the gas film nozzle for atmospheric flames [27]. Combustion air is supplied to the flame through a central (diameter 7.7 mm) and an annular nozzle (inner diameter 9.1, outer diameter 12.4 mm). Both air flows are fed from a common plenum and pass radial swirlers. Fuel is injected between the two air flows through 36 straight channels forming a concentric ring. The combustion chamber measures 124 mm in height and has a square section of 84x84 mm^2 with beveled edges. Four quartz windows 124x69x3 mm^3 are mounted between the four water-cooled copper posts yielding optical access to the flame. Each of the four posts has an additional air duct for the injection of oxidation air into the combustor at a height of 78.5 mm (not shown in figure).

C_2H_4/air flames similar to those described in [28] were used to study the influence of turbulence on laser beam quality at different pressures. Measurements were carried out at 3, 5, 7 and 9 bar with a thermal power of approximately 5 kW/bar. The local equivalence ratio at the nozzle exit was Φ=1.2. An equal amount of oxidation air was added, yielding a global equivalence ratio of Φ=0.6.

3.3 Instantaneous extinction calibration approach applied to technical test case

3.3.1 Optics

The optical setup was similar to that described in [3] and is displayed in Fig. 5. For LII excitation, the fundamental wavelength of a Nd:YAG laser at 10 Hz repetition rate with a pulse duration of 7 ns (Spectra Physics, GCR3-230), was employed. The laser beam was formed into a sheet by a cylindrical f=-200 mm and a spherical f=1000 mm lens and the wings of the sheet exhibiting decreasing laser fluence were clipped by a suitable rectangular aperture. The remaining 30 mm high sheet was attenuated to approximately 35-40 mJ pulse

energy by a half wave plate and a polarizer, yielding a laser fluence not too far beyond the typical LII threshold of approx. 0.3 J/cm^2.

The signals were detected by a double frame image intensified CCD camera (Dicam Pro, PCO). The first gate of 60 ns duration was set before the laser pulse to acquire the background from the flame luminosity and the second gate of same duration started with the laser pulse. The camera was equipped with a pair of filters (LOT 450 FS40-50, LINOS B46) transmitting LII radiation centered at 450 nm.

In addition, the second harmonic (λ=532 nm) of the same laser was formed to a light sheet for extinction measurements quasi-simultaneously with the LII excitation output at 1064 nm. For the extinction measurements, the green laser sheet was attenuated to below 1 mJ while the high power IR beam was delayed by a few meters resulting in a temporal separation of extinction and LII process. The reasons for this are as follows: (1) the strong LII beam is not suitable for an extinction measurement itself due to its potential to change the soot properties thus influencing the absorptive properties on the optical path [23] and (2) a delay prevents measuring extinction information of a partly modified soot distribution. Part of the incident green sheet was deflected onto a quartz cell (in a position comparable to the sheet focus inside the combustor) containing fluorescent dye solution for monitoring the sheet profile. The portion of the green sheet passing the flame is re-imaged onto a second quartz cell adjacent to the first one using a spherical f=250 mm lens with a diameter of 50 mm. Fluorescence emission from the dye cells is monitored by an ICCD camera (Flamestar2, LaVision) synchronized to the LII experiment. The ratio of both fluorescence intensities with sooting flame present, taking into account the respective values with non sooting flame as reference for the optical path, provides the desired extinction information.

3.3.2 Burner

The experiment was performed at the high pressure test rig at the DLR Institute of Combustion Technology, Stuttgart. It features large optical access for laser-based diagnostic techniques up to pressures of 40 bars, while at the same time allowing a wide range of operating conditions, in terms of pressure, preheat temperature, air to fuel ratio, and pressure loss.

The length of the combustion chamber, introduced into the pressure vessel, was 120 mm with a cross section of 85x85 mm^2. The quartz laser ports in the upper and lower chamber wall were 10 mm wide and 120 mm long. Perpendicular to the plane defined by laser sheet excitation large quartz windows provided full optical access to the combustion process. On each of both sides of the combustion chamber, two parallel quartz windows were mounted with a gap between them for guiding cooling air to the back side of the inner one. Secondary air was injected into the combustor through holes in the upper and lower walls 80 mm downstream the injector which strongly decreases the temperature and soot concentrations at the combustor exit. The combustion chamber converges to a circular exit of 50 mm diameter, after that the exhaust gas is guided through a quench to the pressure regulating exit valve. Typical operation was performed at an air temperature of T=630 K.

The principle of the injector was similar to the one described one section before based on the full scale gas film nozzle [27]. Similarly, swirled combustion air was supplied to the flame through a central and an annular nozzle (Fig. 4). In contrast, the fuel, here liquid kerosene, was injected by an air blast nozzle on the injector axis that is placed flush with the burner front panel. Typical operation was moderately lean (very lean after including the oxidation air after two thirds of the combustion chamber) resulting in soot formation due to local rich zones close to spray evaporation.

6

The studied operating condition at 15 bars used 10.76 g/s kerosene and 190 g/s combustion air at 630 K preheat, corresponding to a primary equivalence ratio of Φ=0.83. The resulting pressure drop at the burner inlet was 1.6% relative to the combustor pressure. Additional oxidation air of approximately half the combustion air was injected 80 mm downstream of the injector. This operating point was chosen rather than those at lower pressure because the sufficiently high soot concentrations provide significant attenuation of the laser beams.

4. Results

4.1 Extinction measurements in stable reproducible flame using different wavelengths

Extinction of the laser beam in sooting flames can primarily be caused by scattering of the laser light by particles (Rayleigh/Mie scattering), absorption by molecules and absorption by particles. The contribution of scattering to extinction measurements can be neglected as long as the radius of gyration R_g of the soot aggregate is below the guidance level of $0.7\,\lambda\,/\,(2\pi)$ [29]. Typical diameters of primary soot particles in the investigated or similar flames are clearly below 60 nm [9,10]. Aggregation is weak in the initial phase of soot formation in the type of flame considered here [10] and therefore, in this investigation the contributions from scattering can be neglected. Soot volume fractions determined from extinction measurements at the three different wavelengths according to equation (1) are displayed in Fig. 6 top and Fig. 6 bottom, for the equivalence ratios 2.1 and 2.3, respectively. Error bars include uncertainties in the determination of the absorption length at given HAB and fluctuations of the measured signal levels. For comparison, f_v values from Axelsson et al. [2], measured at an absorption wavelength of 532 nm, are included. For the purpose of comparability, we applied the same refractive index of soot as [2], i.e. m=1.56-0.46*i*, resulting in a dimensionless extinction coefficient of K_e=5.01. We assumed the dimensionless extinction coefficient to be sufficiently independent of wavelength, as supported by Therssen et al. [30]. It should be noted that the exact choice of a single refractive index is not important for the key findings of our experiments.

Determined transmissions I/I_0 were above 0.89. The results reveal a significant discrepancy between the different wavelengths. A comparison with soot volume fractions determined by Axelsson et al. [2] using 532 nm shows a principal agreement of the values but moderate deviations in the exact quantities. This might be due to different methods in determining the optical path length L, differences in ambient pressure or temperature (influencing the real gas flow rates) or to discrepancies in the burner quality and flame homogeneity, as argued by Migliorini et al. [8]. Another source of discrepancy is the chosen procedure of background determination. While in our measurements background was determined without flame, others chose a moderately rich but non sooting flame, a procedure that removes the offset at incipient soot formation. Moreover, the larger relative error bars for the less sooting Φ=2.1 flame indicate a stronger influence of measurement uncertainties for small extinctions. For the weakly sooting flame, accompanied by quite weak beam attenuation even small variations of the mass flows or the environment conditions may have a significant influence on the soot formation.

The qualitative and quantitative absorption behavior for each of the three wavelengths is different: At 532 and 632.8 nm the evaluated soot volume fractions at low HAB are the same but they diverge at higher HAB. Soot volume fractions determined in the infrared are smaller throughout the complete flame. At HAB=4 mm there is almost no soot luminosity in the photos apparent (Fig. 7) in accordance with the extinction measurement in the infrared which shows zero absorption. In contrast, measurements at the shorter wavelengths show a considerable absorption.

If the deviation were solely due to different refractive indices at the different wavelengths, linear scaling of the curves would lead to agreement of the three curves since K_e correlates with the determined soot volume fraction linearly (see eq. 1). However, simple linear scaling of the curves measured at the different wavelengths does not lead to an overlap. Thus a variation of refractive index with wavelength is not sufficient to explain the effect of disagreeing curves. This behavior can rather be explained by non-negligible absorption by soot precursors, i.e. polycyclic aromatic hydrocarbons (PAH), at the absorption wavelengths of 532 and 632.8 nm. Correspondingly, the difference in LII excited at 1064 and 532 nm, respectively, was attributed to PAH in literature [5].

The observed offset between longest and shortest wavelength shows a higher relative contribution for the Φ=2.1 flame, where soot concentrations are lower by a factor of approx. 2.5. Following the above argumentation, this would be linked to a faster increase of soot concentrations in comparison to large PAH with increasing equivalence ratio. Evidence for this statement is not available from literature since species measurements in this type of flame are typically limited to species smaller than for example perylene or benzo(a)pyrene ($C_{20}H_{12}$) [31], corresponding to an absorption wavelength below 450 nm. For the concentrations of those species, there was no general trend observable for different Φ; rather, the studied species behaved differently and a strong dependence on the position in flame was seen. On the other hand, most detailed gas phase kinetic models are developed and optimized for a similar species range of relatively small molecular size or do not account for soot precursor consumption as soot is computed in a post processing loop [32]. Thus, a qualitative statement from the theoretical perspective is not available, too.

4.2 Beam steering in turbulent lab flames at different pressures

Laser diagnostic measurements in turbulent flames using techniques like Rayleigh scattering or OH laser-induced fluorescence easily indicate the occurrence and amount of beam steering present in the single shot images. Here, the gas density or OH distributions are homogeneous over large areas and changes in the signal intensity distributions due to beam steering can well be identified [12,13]. In contrast, soot signatures in turbulent flames are often very limited in size and span a wide dynamic intensity range. This prohibits simple identification of the influence or even presence of beam steering.

Beam steering in turbulent flames is due to density gradients and thus depending on the system pressure and linearly on temperature gradients across the turbulent flame fronts. Another parameter influencing the refractive index is the local gas composition. A more detailed description including the influence of pressure is provided by Weinberg [12]. Fig. 8 presents the intensity profiles of the laser beam recorded by the beam profiler as described above for different pressures. The upper row shows the distributions averaged over 64 shots and the middle row shows representative single shots. The distribution on the left side represents the "reference case", i.e. the distribution without flame at 1 bar. For the averaged images, the profiles integrated in horizontal and vertical directions are also displayed below and left of the images, respectively. The red line displays the profile of the corresponding flame and the black line the reference case. The vertical wave-like shape is due to diffraction effects stemming from the aperture which limits the height of the laser sheet. This feature does not influence the findings described in the following. Regarding the averaged 2D sheet profile, pressure seems to improve the laser beam quality. The reason for a smoothing effect on the shape of the laser sheet is, that statistical beam fluctuations from beam steering homogenize the average local laser fluence. The integrals show that the line integrated intensity is smeared moderately. However, the analysis of single-shot images shows that the opposite of a smoothing effect is present for single shot exposures. The evaluation of the RMS values of the same images (not shown) reveals that without flame the RMS remains low in the

8

entire profile, indicating that the characteristics of the sheet profile remain almost identical from laser-shot to laser-shot. But with flame and especially increasing pressure the RMS values are significantly increased.

The single shot images displayed in the middle row demonstrate that the intensity distribution is more and more disturbed as the pressure is increased. The representation clearly shows that beam profiles must be studied based on the single shots. If the same line integration as above is performed for all single shot images, a broad band of profiles instead of a single one is obtained indicating the variations. Here it is also seen that the variations increase with pressure, as expected. Nevertheless, relative to the average profiles the amplitude of fluctuations remains limited, at least in this integrated representation. Additionally, it can be recognized that the sheet envelope remains almost unchanged, while the profile inside changes significantly. With increasing pressure even the use of a thinner sheet would not result in a spatial resolution better than 1 mm.

An even more detailed view is given in the third row, where the statistics of the local intensity over a complete sequence is plotted for three square locations in the laser sheet (5x5 pixel squares indicated in one second row 2D image). Square locations with equal intensities have been chosen in order to improve the statistics by combining them in one histogram. While without a flame the same intensity is detected in every image of the sequence, the distribution of the local laser fluence broadens with flame and pressure. The main features of this trend are 1) most probable fluence shifts to lower values but remains similar, 2) local fluence variations become more prominent with increasing pressure, 3) certain fluence limits are not exceeded (i.e. approx. ±50% of the original laser beam fluence, averaged over the rectangles). Extrapolation of the fluence distribution to higher pressure levels should be possible. The width of the histograms of the fluence distribution indicates the level of fluctuations and thus shall be helpful to determine a suitable fluence of the incident laser beam for application of LII in order to prevent too low fluence.

The worst case of beam steering effects is detected for the turbulent flame at 9 bars. For this case, an extension of the statistical analysis is given in Fig. 9. Here, images are composed of the local minima and maxima, respectively, of the complete sequence and compared to the averaged sheet profile. Despite the clearly visible beam steering effects (structures, intensity deviations from average), local minima and maxima do not significantly exceed the above mentioned limits of ±50% of the average. Only on a single pixel basis fluctuations between 30% and 200% of the incident values occur. To remain above the lower limit of the plateau regime, a sufficiently high incident laser fluence has to be chosen to account for potential fluence reductions due to beam steering. In our own example referenced in Fig. 1 the LII plateau starts at approximately 0.3 J/cm^2 [26], thus a suitable incident fluence in that case were 0.5 J/cm^2, well accepting that in single cases the local fluence after beam steering can be as high as 1.0 J/cm^2. That has to be taken into account when discussing accuracy of single shot LII quantification, but will not change the time averaged information significantly since unsuitable events occur rarely.

4.3 Instantaneous extinction calibration approach applied to technical test case

The studied calibration approach requires correlation of the attenuated laser beam with an LII image of the complete path where attenuation by soot occurs; in our experiment this condition of full optical access is fulfilled, apart from unavoidable window pollution during combustion. In principle, according to eq. (1) the averaged soot volume fraction f_v can be determined if incident and transmitted beam intensity (I and I_0, respectively) are known, as well as the dimensionless extinction coefficient K_λ and the optical path length L.

The soot volume fraction, on the other hand, is linked to the LII signal integrated on the same optical path

$$f_v = C \int_L LII(y)\, dy \tag{2}$$

by a suitable calibration constant C. The principle is demonstrated in Fig. 10. The left part of the figure shows a representative flame image, the central part is a single shot LII image and on the right the corresponding pair of dye cell images is shown.

For a proper description of the correlation two effects have to be considered: suitable imaging of the diverging laser beam after the combustor onto the dye cells for monitoring of laser attenuation as well as the size and concentration of the soot clouds and the corresponding level of attenuation. Absorption should not be too weak, to be covered by beam steering effects or masked by measurement uncertainties.

To correct for beam steering generated inside the combustor, imaging of the transmitted laser sheet profile from the combustor axis to the detection device was applied. However, only the effect of beam steering events within the depth of the field of this lens can be removed by imaging onto the quartz cell used for monitoring the transmitted beam. Since the depth of the field of this imaging lens was significantly shorter than the combustor diameter and temperature gradients on the laser path can not be localized, an ideal correction for beam steering could not be achieved.

Consequently, a spatially resolved correlation (correlation for each single x in the figure) of attenuation and corresponding integrated LII signal on the same optical path yields a wide scatter not exhibiting any trend at all. Such a correlation would contain values for 64 single optical paths (useful pixel columns) in 200 image pairs. Thus, the deduction of the calibration constant in eq. (2) on a single line basis is not possible.

Fig. 11 displays the correlation for all 200 single laser shots (not spatially resolved). The optical density OD is expressed as

$$OD = -\log\left[\left(\frac{I}{I_0}\right)\left(\frac{I_{0,ref}}{I_{ref}}\right)\right] \tag{3}$$

where the reference intensities represent the detected fluorescence from the dye cells for events without soot; the reference ratio thus describes the different transmittance and detection efficiencies of the two paths. The vertical axis represents the LII line integrals (integrated along the optical path, then averaged in x-direction) while OD is an average of the full laser sheet profile attenuation information (as well averaged in x-direction).

As expected, images containing high LII intensity correlate well with high optical density determined from the transmitted laser beam intensity. For a single optical path a strictly linear behavior according to eq. (1) should result. The slight deviation can be attributed to averaging I, I_0 and the LII signal along all optical paths in each image. Still, a significant scatter of data points is present. We attribute this residual scatter to absorption of species other than soot at the used extinction wavelength of 532 nm. That is in accordance with the findings of the extinction experiments in laminar flames described above. Choice of a different wavelength for this experiment at technical conditions would have been preferable but could not be realized at that time due to test-rig availability and costs.

Another potential source of scatter is the slightly different effective sheet thickness for both diagnostics, leading to slightly different probe volumes. While the full sheet thickness contributes in case of extinction, only those parts of sufficient laser fluence become efficient for LII. This might introduce a bias if species concentrations are not homogeneous along the

sheet thickness. Due to the influence of beam steering, changing the sheet profile along the passage through the flame, this effect cannot be accounted for. Nevertheless, the trend shown in Fig. 11 is suitable for deducing an on-line calibration constant even at these harsh operating conditions without the need of ex-situ calibration of the used LII setup or introducing a calibration flame of known soot concentration at the location of the measurement. This calibration procedure is accounting for changes of LII decay times with pressure relative to the detection gate while changes of optical soot properties with pressure might be included as a next step to deduce a best possible calibration constant.

Note that two conditions are essential for this on-line calibration approach:

-   soot concentrations have to be significant to dominate other effects like beam steering or window pollution of the combustor

-   the full diameter of the flame must be visible in the LII image to monitor all sources of laser beam attenuation on the LII camera

For moderate soot concentrations with their typical small structures of high dynamics, including steep gradients, an excellent alignment of both used laser beams is essential to correlate the correct information.

5. Summary and conclusions

Measurements have been performed in different sooting flames in order to investigate the influence of the wavelength in extinction measurements and beam steering effects in LII both affecting the accuracy of LII measurements. The comparison of absorption measurements performed at 532, 632.8 and 1064 nm in a simple sooting standard flame indicated a significant contribution to absorption at visible wavelengths that cannot be attributed to soot. The absorption is most probably caused by polycyclic aromatic hydrocarbons. Thus, for calibration purposes of LII by absorption the use of a long wavelength is recommended to avoid influence of non-soot absorbents.

The influence of beam steering has been investigated in turbulent flames in a gas turbine model combustor at pressures up to 9 bars. Beam steering at our experimental conditions clearly influences the local fluence of a laser sheet passing the turbulent flames. As expected, the influence of fluctuating temperature gradients within the flame increases with pressure. The local laser fluence varied between 30% and 200% of the incident value in the worst case at 9 bars during our experiments. This demonstrates that a uniform laser profile with a fluence shortly above the LII plateau threshold - as preferably applied in LII measurements - cannot be achieved in turbulent flames. Thus for the applied fluence a compromise must be chosen between too close to the threshold risking to drop locally below this value and too high fluence significantly vaporizing soot particle volume. When choosing laser fluences of approx. 0.5 J/cm^2 and preferably a homogeneous beam profile, the effect of locally fluctuating laser fluences should remain low in practical applications. For the evaluation of the measurement precision, single shot beam profiles have to be checked in detail. Quantitatively, the statistically few events where the laser fluence falls below the threshold locally would hardly change the general information from a full sequence of laser shots. The similar is valid for the few events of very high (local) fluence. Nevertheless, when trying to quantify one single LII image, this statistical probability has to be taken into account when describing precision. On the other hand, a spatial resolution below 1 mm in dimension of the laser sheet thickness is not realistic under technical conditions. However, the described qualitative behavior probably is useful for any technical setup in general, while the quantification of the beam steering influence is strongly dependent on parameters as turbulence, thermal gradient properties, preheat temperature, cooling concept and pressure.

A new LII calibration approach is proposed for technical conditions employing a quasi-simultaneous extinction experiment. This approach was demonstrated for a technical flame at 15 bars. While a spatially resolved correlation of absorption measured at 532 nm and corresponding LII signal was not successful due to beam steering and absorption by PAHs, a correlation on a full image shot-to-shot basis proved applicable. A large variety of different soot concentrations in the single shot LII images correlates almost linearly with the corresponding laser attenuation. As an improvement for the future this approach should use a more suitable infrared wavelength rather than the 532 nm in our actual experiment. The described approach is in principle suitable for technical combustion systems where a calibration flame cannot be mounted at the location of the technical experiment provided full optical access to the flame and sufficiently high soot concentrations are given.

References

[1] H. Bladh, J. Johnsson, P.-E. Bengtsson, Appl. Phys. B **90**, 109 (2008)

[2] B. Axelsson, R. Collin, P.-E. Bengtsson, Appl. Opt. **39**, 3683 (2000)

[3] M.S. Tsurikov, K.P. Geigle, V. Krüger, Y. Schneider-Kühnle, W. Stricker, R. Lückerath, R. Hadef, M. Aigner, Combust. Sci. Technol. **177**, 1835 (2005)

[4] R.L. Vander Wal, T.M. Ticich, Appl. Opt. **38**, 1444 (1999)

[5] C. Schoemaecker Moreau, E. Therssen, X. Mercier, J.F. Pauwels, P. Desgroux, Appl. Phys. B **78**, 485 (2004)

[6] G. Prado, A. Garo, A. Ko, A. Sarofim, Proc. Combust. Inst. **20**, 989 (1984)

[7] C. Schulz, B.F. Kock, M. Hofmann, H. Michelsen, S. Will, B. Bougie, R. Suntz, G. Smallwood, Appl. Phys. B **83**, 333 (2006)

[8] F. Migliorini, S. De Iuliis, F. Cignoli, G. Zizak, Combust. Flame **153**, 384 (2008)

[9] R. Stirn, T. Gonzalez Baquet, S. Kanjarkar, W. Meier, K.P. Geigle, H.-H. Grotheer, C. Wahl, M. Aigner, Combust. Sci. Technol. **181**, 329 (2009)

[10] M.M. Maricq, S.J. Harris, J.J. Szente, Combust. Flame **132**, 328 (2003)

[11] B. Hemmerling, *in Proc. Spie,* M. Tacke, W. Stricker, ed., Vol. 3108 of Combustion Diagnostics (The International Society for Optical Engineering, 1997) 32-37

[12] F. Weinberg, Proc. Combust. Inst. **26**, 939 (1996)

[13] S.A. Kaiser, J.H. Frank, M.B. Long, Appl. Opt. **44**, 6557 (2005)

[14] J.E. Dec, A.O. zur Loye, D.L. Siebers, *SAE Tech. Paper 910224,* Society of Automotive Engineers, Warrendale, Pa., (1991)

[15] B. F. Kock, T. Eckhardt, P. Roth, Proc. Combust. Inst. **29**, 2775 (2002)

[16] S. Schraml, C. Heimgärtner, C. Fettes, A. Leipertz, Proc. 10th Int. Symposium on Applications of Laser Technologies to Fluid Mechanics, Lisbon, Portugal, (2000)

[17] A. Boiarciuc, F. Foucher, C. Mounaim-Rousselle, Appl. Phys. B **83**, 413 (2006)

[18] B. Bougie, L. Ganippa, N.J. Dam, J. Ter Meulen, Appl. Phys. B **83**, 477 (2006)

[19] R. Ryser, T. Gerber, T. Dreier, Combust. Flame **156**, 120 (2009)

[20] T.R. Meyer, S. Roy, V.M. Belovich, E. Corporan, J.R. Gord, Appl. Opt. **44**, 445 (2005)

[21] R.L. Vander Wal, D.L. Dietrich, Appl. Opt. **34**, 1103 (1995)

[22] E. Clar, *Aromatische Kohlenwasserstoffe* (Springer, Berlin, Göttingen, Heidelberg 1952)

[23] R.L. Vander Wal, T.M. Ticich, A.B. Stephens, Appl. Phys. B. **67**, 115 (1998)

[24] H.A. Michelsen, A.V. Tivanski, M.K. Gilles, L.H. van Poppel, M.A. Dansson, P.R. Buseck, Appl. Opt. **46**, 959 (2007)

[25] H. Bladh, P. Bengtsson, J. Delhay, Y. Bouvier, E. Therssen, P. Desgroux, Appl. Phys. B **83**, 423 (2006)

[26] K.P. Geigle, Y. Schneider-Kühnle, M. Tsurikov, R. Hadef, R. Lückerath, V. Krüger, W. Stricker, M. Aigner, Proc. Combust. Inst. **30**, 1645 (2005)

[27] P. Weigand, W. Meier, X.R. Duan, W. Stricker, M. Aigner, Combust. Flame **144**, 205 (2006)

[28] O. Lammel, K.P. Geigle, R. Lückerath, W. Meier, M. Aigner, GT2007-27902, Proc. ASME Turbo Expo 2007: Power for Land, Sea and Air, Montreal (Canada)

[29] M.Y. Choi, G.W. Mulholland, A. Hamins, T. Kashiwagi, Combust. Flame **102**, 161 (1995)

[30] E. Therssen, Y. Bouvier, C. Schoemaecker-Moreau, X. Mercier, P. Desgroux, M. Ziskind, C. Focsa, Appl. Phys. B **89**, 417 (2007)

[31] T. R. Melton, F. Inal, S. M. Senkan, Combust. Flame **121**, 671 (2000)

[32] M. Kamphus, M. Braun-Unkhoff, K. Kohse-Höinghaus, Combust. Flame **152,** 28 (2008), and references therein

Figure captions:

Fig. 1: LII response curves from literature for different experimental conditions as excitation wavelength, spatial averaging, gate duration and delay (see text for details).
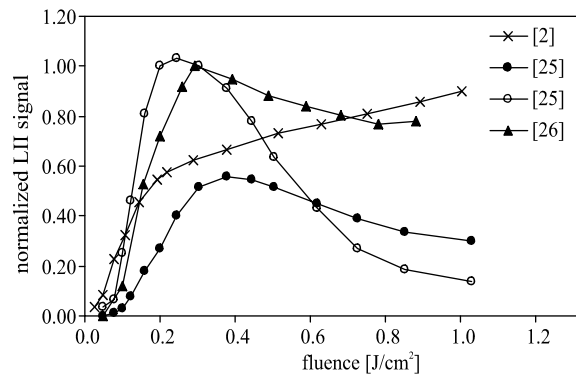
Fig. 2: Experimental setup employed for the absorption measurements at different wavelengths. The chopper was not required for measurements at 1064 nm.
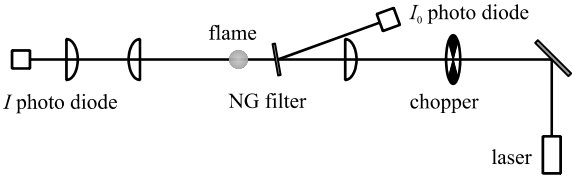
Fig. 3: Experimental setup employed for beam steering studies at different pressures between 1 and 9 bars.
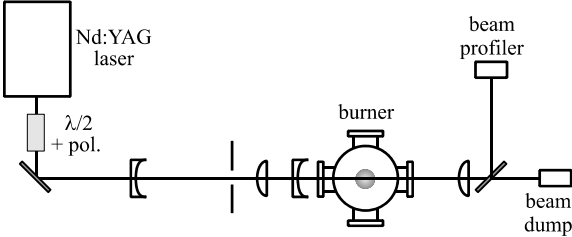
Fig. 4: Schematic of the turbulent lab burner including the main flame features inner and outer recirculation zone (irz, orz), time averaged flame zone and instantaneous flame front as well as the laser sheet.
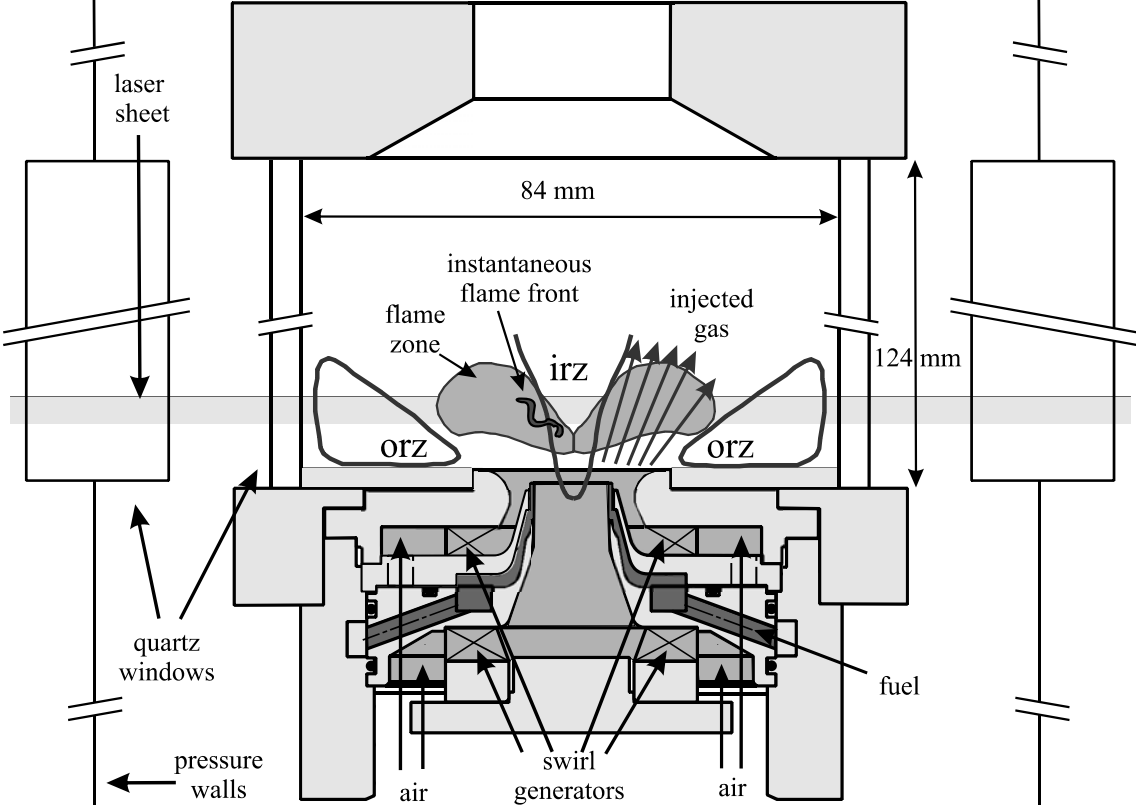
Fig. 5: Experimental setup employed for technical experiment. The IR laser pulse is delayed and significantly stronger compared to the green pulse. Representative images of the two dye cells and a LII image are included.

Fig. 6: Absorption measurements at different wavelengths and comparison with literature [2] for flames at Φ=2.1 (top) and Φ=2.3 (bottom).

Fig. 7: Pictures of the 2 studied premixed laminar C_2H_4/air flames. The stabilization plate is visible in the upper part of the flame while the white and black grid lines, respectively, indicate 2 mm steps above the burner surface.

Fig. 8: Laser profiles at different pressure, averages (top) and representative single shots (center). Integrated profiles are included, black for the reference case without flame at 1 bar and red at the respective pressure (top) while similar profiles in the second row represent the 64 single shot data. The bottom row shows intensity histograms evaluated in the three rectangles inserted in the middle row. Inserted numbers represent the peak location and width of the distributions, including 90% of the events.

Fig. 9: For the 9 bar case the left and right profiles are composed of minimal and maximal single pixel values from the complete sequence in comparison with the pure average profile (center). In addition, intensity profiles at the indicated axis are visualized in the right plot. Note that the left image is dominated by single dark events that might occur only once per sequence.

Fig. 10: Representative picture of the technical flame (left), LII single shot image (center) and dye cell images plus *I* profile as averaged between both red lines (right). The flow direction and position of the green and IR laser sheets are indicated, respectively. Correlation of absorption and LII might be performed spatially resolved in *x*-direction or *x*-averaged. For a spatial resolution along x the LII integral along the indicated gray line is correlated to the local extinction at the same location (gray line in dye cell representation).

Fig. 11: Correlation of absorption represented by optical density (OD) with LII intensity without spatial resolution. 200 dots indicate the 200 single shot data detected at this operating condition of the technical combustor.

Fig. 1: LII response curves from the literature for different experimental conditions as excitation wavelength, spatial averaging, gate duration and delay (see text for details).

Fig. 2: Experimental setup employed for the absorption measurements at different wavelengths. The chopper was not required for measurements at 1064 nm.

Fig. 3: Experimental setup employed for beam steering studies at different pressures between 1 and 9 bars.

Fig. 4: Schematic of the turbulent lab burner including the main flame features inner and outer recirculation zone (irz, orz), time averaged flame zone and instantaneous flame front as well as the laser sheet. The oxidation air injection ports after two thirds of the combustion chamber are omitted for clarity. For the technical experiment the same burner principle was used replacing the ring of fuel holes by a spray lance on the burner axis.

Fig. 5: Experimental setup employed for the experiment in the technical flame. The IR laser pulse is delayed and significantly stronger compared to the green pulse. Representative images of the two dye cells and a LII image are included.

Fig. 6: Absorption measurements at different wavelengths and comparison with literature [2] for flames at Φ=2.1 (top) and Φ=2.3 (bottom).
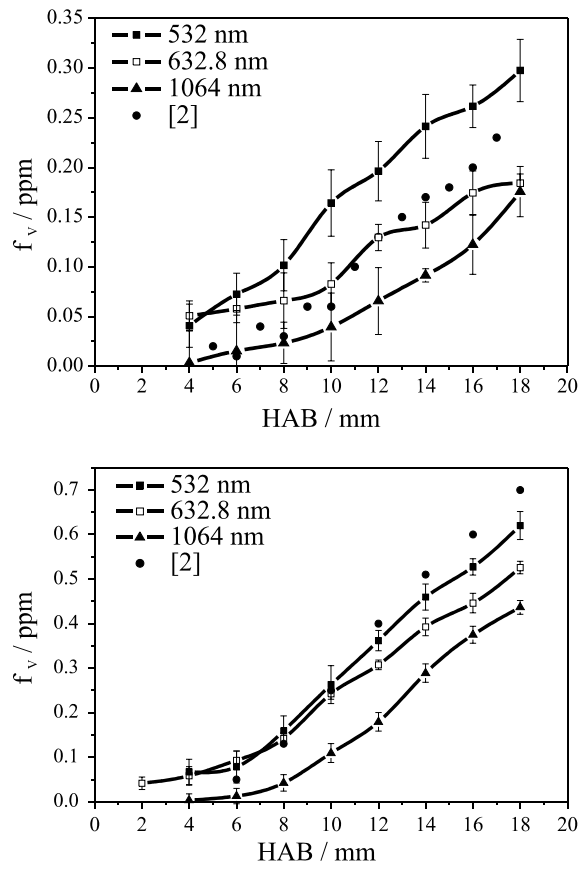
Fig. 7: Pictures of the 2 studied premixed laminar C_2H_4/air flames. The stabilization plate is visible in the upper part of the flame while the white and black grid lines, respectively, indicate 2 mm steps above the burner surface.
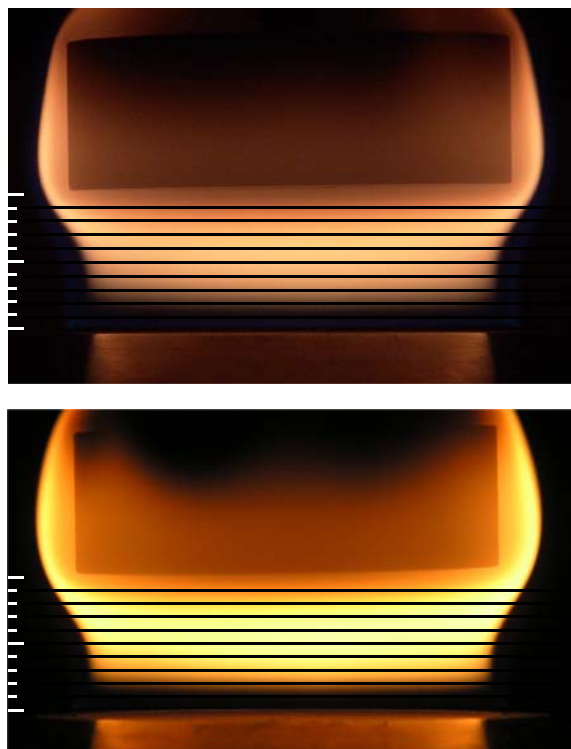
Fig. 8: Laser profiles at different pressure, averages (top) and representative single shots (center). Integrated profiles are included, black for the reference case without flame at 1 bar and red at the respective pressure (top) while similar profiles in the second row represent the 64 single shot data. The bottom row shows intensity histograms evaluated in the three rectangles inserted in the middle row. Inserted numbers represent the peak location and width of the distributions, including 90% of the events.
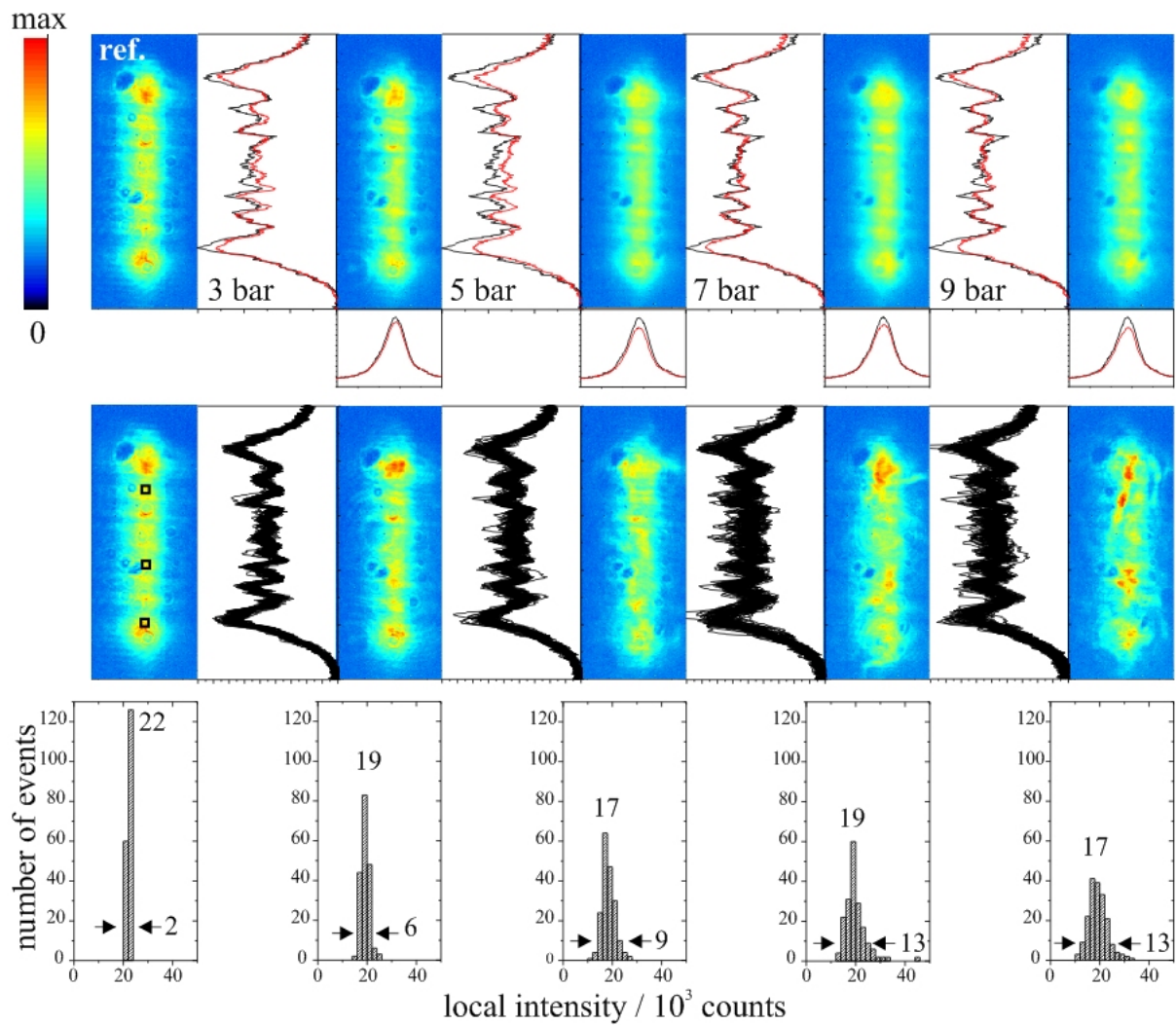
Fig. 9: For the 9 bar case the left and right profiles are composed of minimal and maximal single pixel values from the complete sequence in comparison with the pure average profile (center). In addition, intensity profiles at the indicated axis are visualized in the right plot. Note that the left image is dominated by single dark events that might occur only once per sequence.
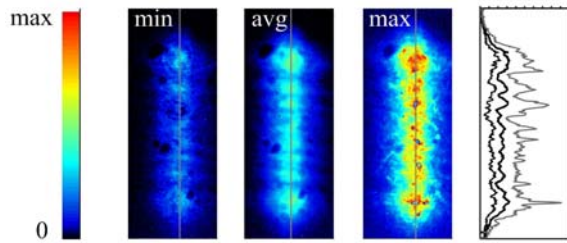
Fig. 10: Representative picture of the technical flame (left), LII single shot image (center) and dye cell images plus *I* profile as averaged between both red lines (right). The flow direction and position of the green and IR laser sheets are indicated, respectively. Correlation of absorption and LII might be performed spatially resolved in *x*-direction or *x*-averaged. For a spatial resolution along x the LII integral along the indicated gray line is correlated to the local extinction at the same location (gray line in dye cell representation).
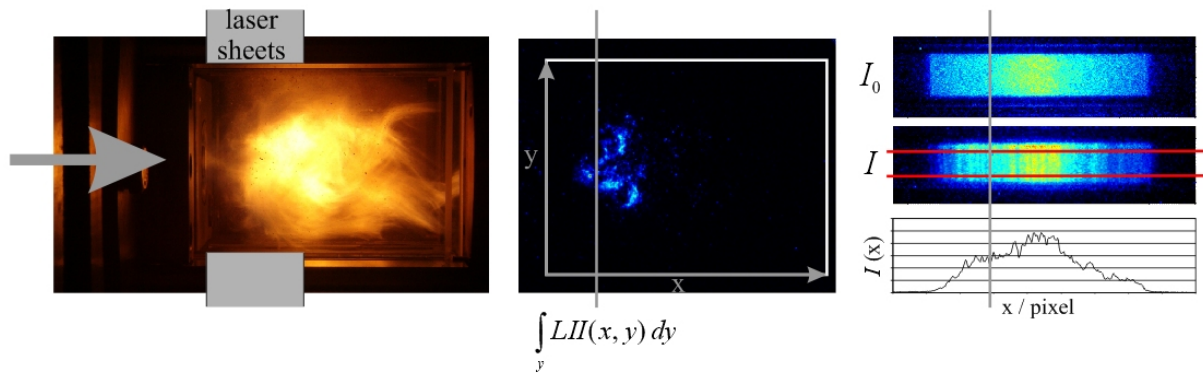
Fig. 11: Correlation of absorption represented by optical density (OD) with LII intensity without spatial resolution. 200 dots indicate the 200 single shot data detected at this operating condition of the technical combustor.